ESR investigation of transition metal defects in $KNbO_3$

1989 J. Phys.: Condens. Matter 1 7267

(http://iopscience.iop.org/0953-8984/1/40/002)

J. Phys.: Condens. Matter 1 (1989) 7267–7276. Printed in the UK

ESR investigation of transition metal defects in $KNbO_3$

E Possenriede, O F Schirmer, H J Donnerberg and B Hellermann
Fachbereich Physik, Universität Osnabrück, Barbarastr. 7, D-4500 Osnabrück, Federal Republic of Germany

Received 10 March 1989, in final form 30 May 1989

Abstract. Using ESR, we identified Fe^{3+} in the rhombohedral phase of the photorefractive compound $KNbO_3$. Fe^{3+}–V_O was found in the orthorhombic as well as the rhombohedral phases. The spectra were analysed and compared to those of Fe^{3+} and Fe^{3+}–V_O in other oxide compounds, e.g. $BaTiO_3$. A superposition model analysis yielded information on the geometry of Fe^{3+} and its nearest neighbours. Also Co^{2+}, Co^{2+}–V_O and Ir^{4+} were identified, analysed and compared to corresponding findings in other oxide hosts.

1. Introduction

Potassium niobate ($KNbO_3$) is among those oxide materials that respond to light-induced space charges by large changes in the refractive index. The crystals thus are well suited for photorefractive applications [1]. Impurities in such materials generally furnish the levels in the bandgap from which charge carriers can be excited to the neighbouring bands, where they move out of the illuminated crystal regions, forming space charges. The knowledge of the properties of defects in $KNbO_3$ is thus essential for understanding their role in sensitising the photorefractive effect. Fe has been found to induce the photorefractive efficiency of $KNbO_3$ especially well, as in comparable compounds such as $BaTiO_3$ and $LiNbO_3$. However, little is known about the microscopic structure of Fe impurities in $KNbO_3$, nor about other lattice defects. Fe^{3+} has been identified in this compound, using ESR, by Siegel [2] and by Siegel and co-workers [3] for the room-temperature orthorhombic phase. A superposition model analysis [4] has led to a detailed picture of the defect structure. Recently, Ti^{4+} has been found to lead to light-induced hole trapping in $KNbO_3$ [5].

$KNbO_3$ shows the same sequence of lattice phases as $BaTiO_3$. Readily accessible to ESR studies are the orthorhombic phase (from about 260 K to about 500 K) and the rhombohedral phase (below about 260 K) [6]. In this paper we describe the identification and analysis of Fe^{3+}, Fe^{3+}–V_O, Co^{2+}, Co^{2+}–V_O and Ir^{4+} in the low-temperature phase. The presence of more than one Fe-containing defect, similar to the case of $BaTiO_3$ [7, 8], indicates that the photorefractive effect might be more involved in $KNbO_3$ than in, e.g., $LiNbO_3$, where only a change of charge from Fe^{2+} to Fe^{3+} (and *vice versa*) takes place.

2. Experimental procedures

The Fe-doped crystals were grown by a top-seeded high-temperature solution technique. The composition of the melt was 53 mol% K_2O to 47 mol% Nb_2O_5. Iron was added in

0953-8984/89/407267 + 10 $02.50

the form of Fe_2O_3. Most of our investigations were made with a specimen containing 150 ppm Fe in the crystal.

The other crystals were grown on a platinum wire lowered into the melt without a seed crystal. Here, the single crystal parts of the specimens were considerably smaller than in those crystals grown by the previous method.

The crystals were doped by adding the corresponding transition metal oxides to the melt. The Co-doped crystal contained 2500 ppm Co in the melt, obtained by the addition of Co_3O_4. The specimen containing Ir was pulled from an iridium crucible. The IrO_2 forming on the crucible walls apparently was dissolved in the melt.

The ESR measurements were performed on a Bruker 200D SRC spectrometer at 9.1 and 34.0 GHz. Cooling was achieved using an Air Products Helitran refrigerator.

3. Fe^{3+}

Since Fe is among the most abundant unintentional dopings in oxide crystal growth, and because Fe^{3+} generally dominates the ESR spectra of such materials, it is necessary to identify the ESR of Fe^{3+} in all crystal phases of $KNbO_3$ before turning to the elucidation of additional resonances.

First we report on the identification of the ESR of Fe^{3+} in the orthorhombic phase (295 K). At 9 GHz these spectra are rather complex, because the axial field splitting [2] is comparable to the microwave quantum. We therefore employed 34 GHz microwaves and the corresponding higher magnetic fields. Under this condition the Zeeman effect dominates the crystal field splitting and the spectra become rather simple (figure 1). A full diagonalisation of the spin Hamiltonian

$$H = \mu_B \mathbf{B}\mathbf{g}\mathbf{S} + \tfrac{1}{6}a[S_x^4 + S_y^4 + S_z^4 - \tfrac{1}{5}S(S+1)(3S^2+3S-1)] + D[S_{z'}^2 - \tfrac{1}{3}S(S+1)] + E(S_{x'}^2 - S_{y'}^2) + \tfrac{1}{180}F[35S_{z'}^4 - 30S(S+1)S_{z'}^2 + 35S_{z'}^2 - 6S(S+1) + 3S^2(S+1)^2]$$

yielded the parameters given in table 1 by fitting to the experimental line positions. Figure 2 shows a simulation of the angular dependence of these positions compared to the experimental results. It is also seen that some $\Delta m = \pm 2, \pm 3$ transitions have been identified. Several lines could not yet be assigned.

In the low-temperature rhombohedral phase of $KNbO_3$, Fe^{3+} had not previously been investigated. Spectra taken at 9 GHz are rather simple in this phase (figure 3). The assignment of the lines is indicated. In the crystal studied, two domains of nearly equal volume were present. Not all allowed transitions could be identified because of the large widths of some of the corresponding lines. The Hamiltonian used for the description of the spectra is

$$H = \mu_B \mathbf{B}\mathbf{g}\mathbf{S} + D[S_{z'}^2 - \tfrac{1}{3}S(S+1)] + \tfrac{1}{6}a[S_x^4 + S_y^4 + S_z^4 - \tfrac{1}{5}S(S+1)(3S^2+3S-1)].$$

The parameters leading to the best fit (figure 4) are $g = 2.001$, $D = \mp 0.0248\ \mathrm{cm}^{-1}$, $a = \pm 0.0121\ \mathrm{cm}^{-1}$. While the value of a is comparable to that of Fe^{3+} in $BaTiO_3$, D is about ten times higher for $KNbO_3$.

From a superposition-model analysis of D (see Appendix) it is derived that Fe^{3+} in rhombohedral $KNbO_3$ remains centred in the cage of the surrounding O^{2-} ions. This is in accordance with previous results obtained by Siegel and Müller [4] for Fe^{3+} in

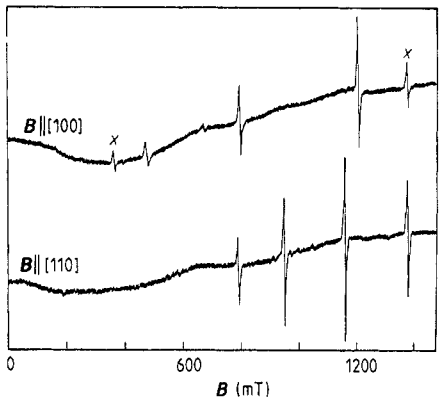

Figure 1. ESR of $KNbO_3:Fe^{3+}$ (orthorhombic phase), $\upsilon = 34$ GHz, $T = 295$ K. The origin of the lines marked x could not yet be identified. They do not belong to Fe^{3+}.

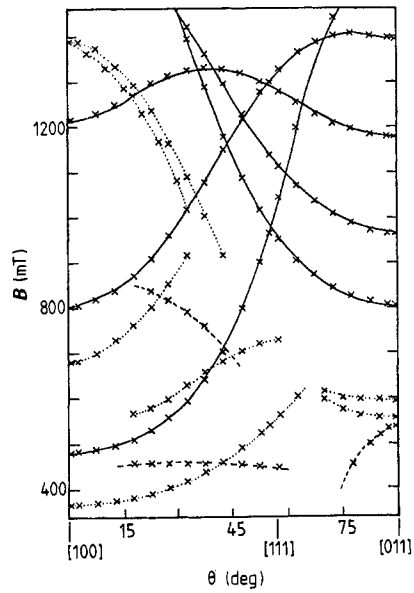

Figure 2. Angular dependence of the line positions of Fe^{3+} in orthorhombic $KNbO_3$, see figure 1. Full curves: $\Delta m_s = \pm 1$ transitions of a single domain. Dashed lines connect the positions of the $\Delta m_s = \pm 2, \pm 3$ transitions. Dotted curves: the resonances could not yet be assigned.

Table 1. Fe^{3+} in $KNbO_3$.

	$T = 20$ K	$T = 295$ K
g	2.0010 ± 0.0020	2.0010 ± 0.0020
D (cm^{-1})	∓0.0248 ± 0.0010	∓0.1752 ± 0.0020
a (cm^{-1})	±0.0121 ± 0.0010	±0.0094 ± 0.0020
E (cm^{-1})	—	±0.0113 ± 0.0020
F (cm^{-1})	—	±0.0001

orthorhombic $KNbO_3$ and in several phases of $BaTiO_3$. Fe^{3+} is repelled by the surrounding O^{2-} ions since the half filled d shell prevents the approach of the ligand valence electrons. This interaction is absent for Ti^{4+} or for Nb^{5+}, where no outer d orbitals are occupied.

It is interesting to note that the experimental result for D can only be understood if a very small angular distortion is taken into account. The polar angle θ (between Z direction and direction to nearest O^{2-} neighbours) is changed from its intrinsic value, 54.62° to 54.45°.

4. Fe^{3+}–V_O

In addition to the signals of isolated Fe^{3+}, other axial ESR spectra were found from Fe-doped $KNbO_3$. They can be ascribed to Fe^{3+} neighbouring an oxygen vacancy, V_O.

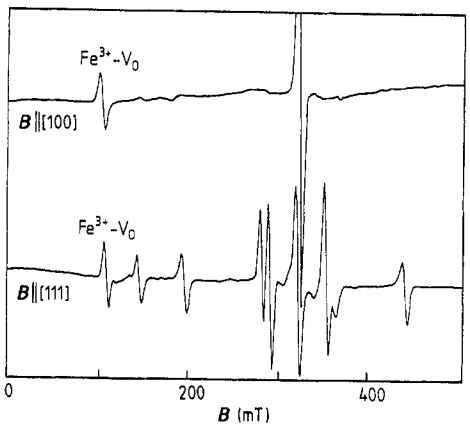

Figure 3. ESR of $KNbO_3:Fe^{3+}$ (rhombohedral phase), $\nu = 9.1$ GHz, $T \simeq 20$ K. Assignment of lines according to figure 4. Resonances of Fe^{3+}–V_O are indicated.

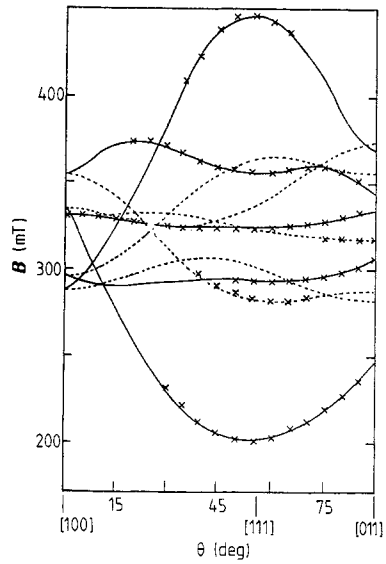

Figure 4. Angular dependence of the line positions of Fe^{3+} in rhombohedral $KNbO_3$, see figure 3. Full curves: $\Delta m_s = \pm 1$ transitions in largest domain. Dashed curves: same in smaller domain.

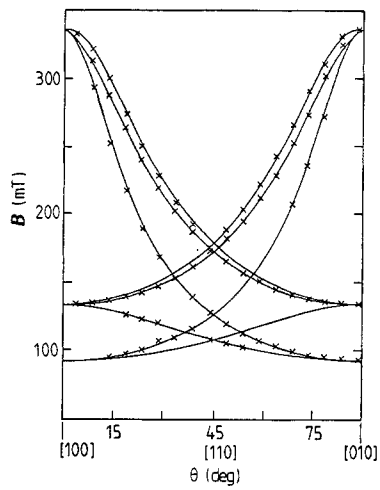

Figure 5. Angular dependence of the line positions of Fe^{3+}–V_O in orthorhombic $KNbO_3$.

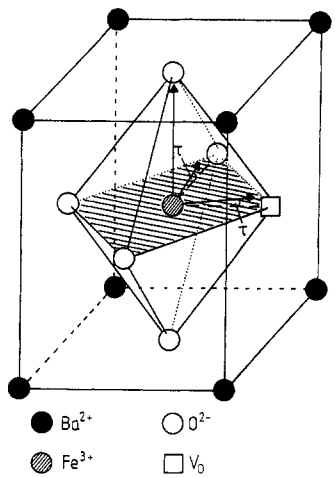

Figure 6. Model of Fe^{3+}–V_O in orthorhombic $KNbO_3$. The arrows indicate the principal directions of the g-tensor.

The corresponding angular plot is given in figure 5. The spectrum is strongly angular dependent with a **g**-tensor characteristic for Fe^{3+} in a strong axial field, $\mathbf{g}_{\text{eff},\parallel} \simeq 2$, $\mathbf{g}_{\text{eff},\perp} \simeq 6$ [9], described by $H = \mu_B \boldsymbol{B} \mathbf{g}_{\text{eff}} S$. Here we find:

$g_{\text{eff},1} = 1.940 \pm 0.010$ $\quad g_{\text{eff},2} = 7.035 \pm 0.005$ $\quad g_{\text{eff},3} = 4.865 \pm 0.005$

with a tilting of $\tau = 1.4° \pm 0.2°$ in a (100)-type plane. This distortion, resulting from the

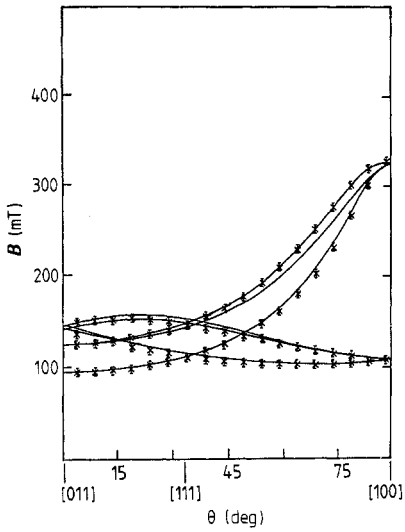

Figure 7. Angular dependence of the line positions of Fe^{3+}–V_O in rhombohedral $KNbO_3$, see figure 3.

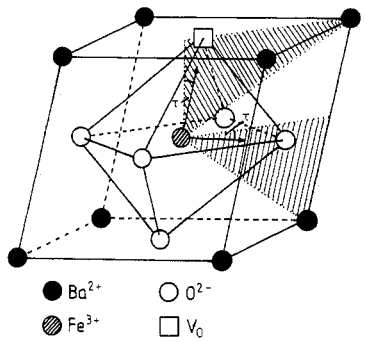

Figure 8. Model of Fe^{3+}–V_O in rhombohedral $KNbO_3$. The principal directions of the g-tensor are tilted in the hatched (110)-type planes.

superposition of the influences of the orthorhombicity of the crystal and the geometry of the Fe^{3+}–V_O pair, causes the splitting of some lines. Figure 6 shows a model of Fe^{3+}–V_O in orthorhombic $KNbO_3$. By measurements at 9 GHz and at 34 GHz, the magnitude of D was determined [9]: $|D| = (1.15 \pm 0.05)\ cm^{-1}$. The orthorhombicity is: $E = (0.053 \pm 0.005)\ cm^{-1}$ [10]. $|D|$ is thus found to be smaller than for Fe^{3+}–V_O in $SrTiO_3$ [9] or in $KTaO_3$ [11]. The axial centre described in [3], having $|D| = (0.73 \pm 0.07)\ cm^{-1}$ can be excluded as arising from Fe^{3+}–V_O because of its small $|D|$.

In the rhombohedral phase the **g**-tensor is

$$g_{\mathrm{eff},1} = 1.99 \pm 0.02 \qquad g_{\mathrm{eff},2} = 6.79 \pm 0.02 \qquad g_{\mathrm{eff},3} = 5.14 \pm 0.02.$$

The corresponding angular plot is given in figure 7. In fitting the line positions a tilting $\tau = 1.6°$ was assumed. Since the signals have rather large linewidths, τ cannot be fixed exactly. Smaller τ, down to 0°, are also possible. An orthorhombic distortion is expected from the superposition of the influences of V_O and the trigonal rhombohedral distortion (figure 8). The value of D could not yet be determined, since the corresponding signals were not identified at 34 GHz. Using the results of [10] one finds from **g**

$$|E/D| = 0.033 \pm 0.003.$$

The analysis of the parameters D and E using the superposition model yields the following results:

(i) In the orthorhombic phase Fe^{3+} moves towards V_O by about 0.2 Å and the O_2^- ions equatorially neighbouring Fe^{3+} move inwards by about 0.1 Å.

(ii) For the rhombohedral phase it is found that, in addition to the values obtained for the orthorhombic phase, the polar angle θ changes by about 1°. It is open whether the intrinsic angle (89.83°) is increased or lowered by this amount.

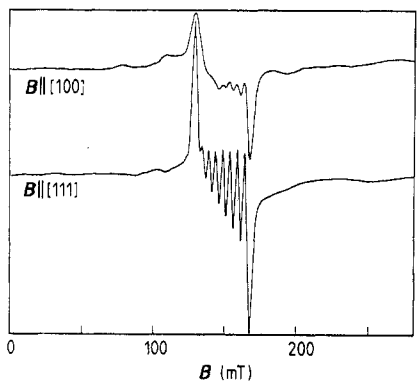

Figure 9. ESR of Co^{2+} in rhombohedral $KNbO_3$ ($T \simeq 20$ K, $\nu = 9.1$ GHz).

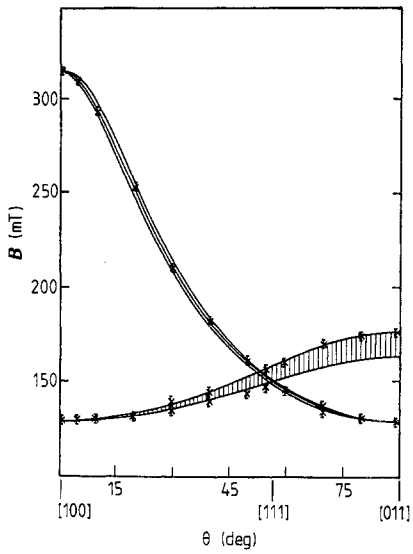

Figure 10. Angular dependence of the line positions of Co^{2+}–V_O in rhombohedral $KNbO_3$, see figure 11. In the hatched region the overlap of the two hyperfine packets could not be disentangled.

5. Co^{2+}

The Co-doped $KNbO_3$ crystals were investigated in the rhombohedral phase at 20 K. An isotropic spectrum was observed, assigned to isolated Co^{2+}, and a strongly angular dependent one, Co^{2+}–V_O. It is interesting to note that the latter was not found shortly after the crystal growth but only during a second investigation about two months later. Apparently oxygen vacancies were diffusing towards Co during that period.

Figure 9 shows spectra of Co^{2+} for $\boldsymbol{B} \parallel [100]$ and [111], respectively. The centroid of the ESR spectrum, as well as the total width of the hyperfine pattern, due to ^{59}Co ($I = \frac{7}{2}$, 100% abundant) is independent of angle. The hyperfine lines are best resolved for $\boldsymbol{B} \parallel [111]$.

The spectrum is described by $H = \mu_B g \boldsymbol{BS} + \boldsymbol{AIS}$ ($S_{\text{eff}} = \frac{1}{2}, I = \frac{7}{2}$) with $g = 4.33 \pm 0.02$ and $A = (0.0101 \pm 0.0002)\ \text{cm}^{-1}$. The groundstate of Co^{2+} in octahedral oxygen environment is $^4T_1$. Spin–orbit coupling of the $S = \frac{3}{2}$ total spin to the effective angular momentum $L = 1$, described by the operator $H_{LS} = \alpha k \lambda LS$ (k orbital reduction, α translation factor), leads to a ground state $J = \frac{1}{2}$, which has to be identified with $S_{\text{eff}} = \frac{1}{2}$. The spectroscopic splitting factor is predicted to be

$$g = [2J(J+1)]^{-1}\{\alpha k[J(J+1) + L(L+1) - S(S+1)] + g_S[J(J+1) + S(S+1) - L(L+1)]\}.$$

With $L = 1$ and $J = \frac{1}{2}$, one obtains $g = (5g_S - 2\alpha k)/3$. Inserting $g_S = 2$ and $\alpha = -\frac{3}{2}$ [12] $g = (10 + 3k)/3$ is found. The experimental result is reproduced with $k = 1$.

This is rather surprising, since in sixfold cubic oxygen environment $k \simeq 0.8$ is found generally for 3d ions. We think that the expected decrease of g is compensated by spin–

Table 2. Co^{2+}–V_O in $KTaO_3$ and $KNbO_3$

	$KTaO_3$	$KNbO_3$
$g_\parallel$	2.061 ± 0.002	2.056 ± 0.005
$g_\perp$	4.933 ± 0.008	5.020 ± 0.010
A (cm^{-1})	0.0057 ± 0.0001	0.0063 ± 0.0002
B (cm^{-1})	0.0074 ± 0.0001	0.0099 ± 0.0002
x	8.57	8.76 ± 0.01
Δ (cm^{-1})	−1100 ± 100	−1156 ± 110
$\lvert P\rvert$ (cm^{-1})	0.021	0.025
κ	0.29	0.26

orbit admixture of higher orbitals. This contribution, not included here, is expected to be positive [13].

6. Co^{2+}–V_O

With the same crystal, ESR spectra were identified similar to those attributed previously to Co^{2+}–V_O in $KTaO_3$ [14]. The angular dependence of the line positions (figure 10) is reproduced by

$$H = \mu_B \boldsymbol{B}\mathbf{g}_{\text{eff}}\boldsymbol{S} + \boldsymbol{IAS} \qquad (S = \tfrac{1}{2})$$

using the principal values of **g** given in table 2. A tilting of the principal axes of **g** by $\tau = 0.9° \pm 0.2°$ as in figure 8 was clearly identified, see figure 10. The experimental line positions in that figure were taken from the centroids of the hyperfine packets; the error bars mark the uncertainties in locating them.

In addition to the spin–orbit coupling, see above, the Co^{2+} cubic crystal-field ground-state, $^4T_1$, now is exposed to a strong axial field

$$H = \Delta(1 - L_z^2) + \alpha' k\lambda LS.$$

In the following we abbreviate $\alpha' k$ by α.

Diagonalisation of this operator leads to the following relation between the components of the **g**-tensor [13]

$$\frac{g_\parallel - 2}{g_\perp} = \frac{(\alpha + 2)3/x^2 - 4/(x + 2)^2}{1 + 2\alpha/(x + 2) + 12/x(x + 2)}.$$

To be in line with the evaluation of Hannon [14] of Co^{2+}–V_O in $KTaO_3$, we assume $\alpha = 1.4$; possibly, this quantity can be somewhat smaller [15]. The auxiliary parameter x describes the results of the diagonalisation in a rational way [13]. Inserting the experimental values of $g_\parallel$ and $g_\perp$, a value for x similar to that of $KTaO_3$ is obtained (table 2).

Using this value, the axial crystal-field splitting Δ can be calculated using $\lambda(Co^{2+}) = 160\ cm^{-1}$

$$\Delta = \lambda\alpha[(x + 3)/2 - 3/x - 4/(x + 2)].$$

The result is included in table 2. In addition, the parameters describing the orbital and core polarisation parts of the hyperfine interaction are seen to be similar to those of $KTaO_3$:(Co^{2+}–V_O).

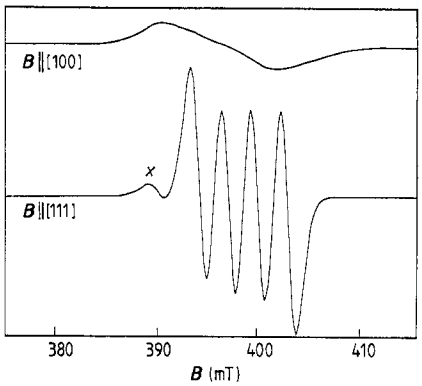

Figure 11. ESR of Ir^{4+} in rhombohedral $KNbO_3$ ($T \approx 20$ K, $\upsilon = 9.1$ GHz). The line marked x could not yet be assigned.

Table 3. Parameter of Ir^{4+} in various oxide hosts.

	$-g_{av}$	k	$-A$ (cm^{-1})	d (Å)	Ref.
$SrTiO_3$	1.604	0.70	0.0024	1.95	18
$KNbO_3$	1.661	0.75	0.0022	2.01	—
MgO	1.738	0.80	0.0026	2.10	16
CaO	1.776	0.83	0.0026	2.35	19
CdO	1.779	0.83	0.0027	2.35	19

7. Ir^{4+}

This charge state of Ir has a characteristic signature both because of its hyperfine interaction and of its g-value. Ir has two stable isotopes; both have $I = \frac{3}{2}$ and nearly identical nuclear magnetic moments. Accordingly, hyperfine patterns of four nearly equally spaced component lines are observed from Ir^{4+} [16]. The $5d^5$ configuration of Ir^{4+} has a strong field $^2T_2$ ($\tilde{L} = 1$) ground state in sixfold cubic oxygen surroundings, which is split by strong spin–orbit coupling into a lower doublet separated from an excited quartet by about 4800 cm^{-1} in a cubic oxygen environment. The g-value thus is constructed similarly to that of alkali atoms in a spin ($s = \frac{1}{2}$)-orbit ($l = 1$) doublet state

$$g = -\tfrac{1}{3}(g_S + 4k)$$

(k orbital reduction). Since $k < 1$, $|g|$ is expected to be somewhat smaller than 2.

These features are found in the spectra shown in figure 11, obtained from a $KNbO_3$ crystal pulled from an Ir crucible. The characteristic hyperfine interaction is best resolved for $\boldsymbol{B} \parallel [111]$. At other orientations several hyperfine packets apparently interfere destructively.

The spectra are described by the Hamiltonian $H = \mu_B \boldsymbol{B}\mathbf{g}\boldsymbol{S} + \boldsymbol{SAI}$, $\mathbf{g}$ being axially symmetric around [111]

$$g_\parallel = -1.651 \pm 0.005 \qquad g_\perp = -1.666 \pm 0.005.$$

The hyperfine interaction along [111] is $A_{[111]} = -(0.0022 \pm 0.0002)$ cm^{-1}. It is seen in table 3 that the average g is explained with $k = 0.75$. It should be noted that this must be considered as an upper bound, since admixtures of excited orbital states [17], not considered explicitly here, tend to increase g. Comparison of the g-values of Ir^{4+} in

several oxide hosts (table 3) indicates that k, and thus also $|g|$, decreases when the Ir–O distance in sixfold cubic oxygen environment decreases. This, of course, is caused by increasing delocalisation of the Ir^{4+} d orbitals. The axiality of **g** is caused by the slight trigonal distortion of the $KNbO_3$ structure in the rhombohedral phase.

The Ir^{4+} signals are rather strong. Apparently, Ir is easily incorporated into $KNbO_3$ from the crucible walls during crystal growth. Thus it is not advisable to use Ir crucibles if pure $KNbO_3$ crystals are desired.

Acknowledgments

We thank Dr H Hesse for initiating the $KNbO_3$ crystal growth and for very useful advice. The maintenance of the ESR laboratory by T Dollinger and W Koslowski and their expert experimental assistance is gratefully acknowledged. The work reported here was supported by DFG, Sonderforschungsbereich 225.

Appendix. Superposition model analysis of the environment of Fe^{3+} and Fe^{3+}–V_O in $KNbO_3$

The experimentally determined parameters D (for Fe^{3+}) and D and E (for Fe^{3+}–V_O) can be interpreted with respect to the distortion of their environments using the Newman [20] superposition model.

The dependence of the crystal-field parameter D on the distance R_i to the N individual ligands i is given by the superposition

$$b_2^0 = \bar{b}_2(R_0) \sum_i^N \left(\frac{R_0}{R_i}\right)^{t_2} \tfrac{1}{2}(3\cos^2\theta_i - 1).$$

Note that $D = b_2^0$. Here $\bar{b}_2(R)$ and t_2 are parameters empirically determined by uniaxial stress experiments on $MgO:Fe^{3+}$ for distances R_i close to the reference distance $R_0 = 2.10$.

Using this relation Müller and Siegel [4] have shown that Fe^{3+} remains centred in the cage of the surrounding O^{2-} ions in orthorhombic $KNbO_3$, unlike the replaced Nb^{5+}. This is due to the population of the 3d orbitals in Fe^{3+}, preventing approach of the O^{2-} ligands.

As discussed by Müller [21] sgn $(a) = +1$ for Fe^{3+} in $BaTiO_3$ and $KNbO_3$. As shown above, sgn $(a) = -$sgn (b_2^0) is found experimentally and therefore $b_2^0 = -0.0248\ cm^{-1}$.

This value cannot be reproduced for the following distortions of the environment of Fe^{3+}: off-centre movement of Fe^{3+} along the axis of the trigonally distorted octahedron; or, alternatively, change of the distances to the O^{2-} ligands while remaining centred. Only slight changes of the polar angle θ_i can explain the experimental b_2^0. Figure A1 shows that the centred position ($\Delta = 0$) and $\theta_i = 54.45°$ lead to agreement. Note that rather minute changes of θ_i from the intrinsic value of 54.62° lead to this result.

For Fe^{3+}–V_O in orthorhombic $KNbO_3$ the four equatorial O^{2-} ions are found to move inward by about 4% ($\simeq$0.1 Å) while Fe^{3+} moves towards the oxygen vacancy by about 0.2 Å. The orthorhombic part of the crystal field, b_2^2, turns out to be rather small, as observed.

In rhombohedral $KNbO_3$, where b_2^0 could not yet be measured, this parameter was taken to be $\simeq 1.1\ cm^{-1}$. This value has been determined for Fe^{3+}–V_O in rhombohedral

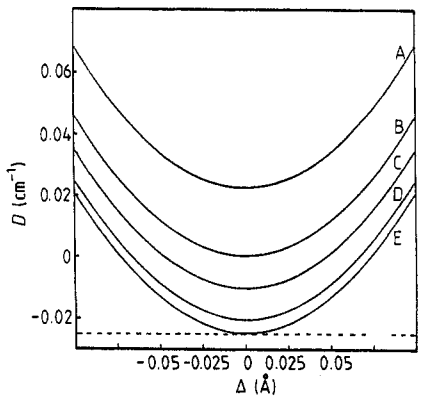

Figure A1. Prediction of crystal field parameter D of Fe^{3+} in rhombohedral $KNbO_3$ according to the superposition model, using the parameters given in the text. The abscissa indicates the off-centre movement of Fe^{3+} along the trigonal axis of the cage of the surrounding O^{2-} ions. Different curves belong to various polar angles (θ) defining the directions on which the O^{2-} ligands are lying: A, 55°; B, 54.74°; C, 54.616°; D, 54.50°; E, 54.45°. The experimental D-value is indicated by the broken line.

$BaTiO_3$ [7] and for orthorhombic $KNbO_3$ (see above). It is found that b_2^0 is sensitive to the inward movement of the equatorial O^{2-}; and b_2^2, to changes of the polar angle θ. Again, the former movement is about 4%, whereas θ varies by about 1°. Since the sign of E could not be determined, the sense of this angular change is open so far. Assuming that the off-centre movement of Fe^{3+} is again 0.2 Å, the ratio $|E/D| = |b_2^2/3b_2^0|$ is predicted to be about 0.033, identical to the experimental value.

References

[1] Günter P and Huignard J-P (ed.) 1988 *Photorefractive Materials and their Applications* (Berlin: Springer)
[2] Siegel E 1976 *Ferroelectrics* **13** 385
[3] Siegel E, Urban W, Müller K A and Wiesendanger E 1975 *Phys. Lett.* **53A** 415
[4] Siegel E and Müller K A 1979 *Phys. Rev.* B **20** 3587
[5] Possenriede E, Hellermann B and Schirmer O F 1988 *Solid State Commun.* **65** 31
[6] Hewat A W 1973 *J. Phys. C: Solid State Phys.* **6** 2559
[7] Possenriede E, Schirmer O F, Donnerberg H J, Godefroy G and Maillard A 1989 *Ferroelectrics* at press
[8] Possenriede E, Schirmer O F, Godefroy G and Maillard A 1988 *SPIE Proc.* Vol 1018 *Electro-Optic and Magneto-Optic Materials (1988)*
[9] Kirkpatrick E S, Müller K A and Rubins R S 1964 *Phys. Rev.* A **135** 88
[10] Holton W C, de Wit M, Estle T L, Dischler B and Schneider J 1968 *Phys. Rev.* **169** 359
[11] Wessel G and Goldick H 1968 *J. Appl. Phys.* **39** 4855
[12] Abragam A and Bleaney B 1970 *Electron Paramagnetic Resonance of Transition Ions* (Oxford: Clarendon)
[13] Abragam A and Pryce M H L 1951 *Proc. R. Soc.* A **206** 173
[14] Hannon D M 1971 *Phys. Status Solidi* b **43** K21
[15] Donnerberg H J and Schirmer O F 1987 *Solid State Commun.* **63** 29
[16] Suss J T, Low W and Foguel M 1970 *Phys. Lett.* **33A** 14
[17] Thornley J H M 1968 *J. Phys. C: Solid State Phys.* **1** 1024
[18] Schirmer O F, Förster A, Hesse H, Wöhlecke M and Kapphan S 1984 *J. Phys. C: Solid State Phys.* **17** 1321
[19] Andlauer B, Schneider J and Tolksdorf W 1976 *Phys. Status Solidi* b **73** 533
[20] Newman D J 1971 *Adv. Phys.* **20** 197
[21] Müller K A 1976 *Phys. Rev.* B **13** 3209